

Collisional stopping power of ions in warm dense matter

Lucas Babati,¹ Shane Rightley,² Nathaniel Shaffer,³ and Scott Baalrud¹

¹*Nuclear Engineering and Radiological Sciences, University of Michigan, Ann Arbor, Michigan, 48109, USA*

²*Sandia National Laboratory, Albuquerque, New Mexico, 87123, USA*

³*Laboratory for Laser Energetics, University of Rochester, Rochester, New York, 14623, USA*

(Dated: November 13, 2025)

A model for the collisional stopping of ions on free electrons in warm dense matter is developed and explored. It is based on plasma kinetic theory, but with modifications to address the warm dense matter regime. Specifically, it uses the Boltzmann-Uehling-Uhlenbeck kinetic equation to incorporate effects of Fermi degeneracy of electrons. The cross section is computed from quantum scattering of electrons and ions occurring via the potential of mean force derived from an average atom model, which incorporates effects of strong Coulomb correlations. Predictions from this model show comparable accuracy to results from time-dependent density functional theory calculations for deuterium near solid density and a temperature of several electronvolts, at a fraction of the computational cost. Further, the model captures the transition of a plasma from the classical limit to the degenerate limit, including qualitative behaviors of solid state theory.

I. INTRODUCTION

The stopping of ions in various materials is a common and well understood problem in many areas of physics [1, 2]. In plasma physics, the study of stopping power has shown increased importance in the effort for fusion energy using inertial-confinement fusion (ICF) [3]. In ICF, energetic charged particles must deposit the energy gained from a fusion reaction, or from a particle beam, into the burning plasma to promote more reactions [4, 5]. This energy transfer is almost entirely due to a drag force the charged particles experience from the surrounding plasma. Accordingly, accurately modeling stopping power in materials relevant to ICF is important for predicting the behavior of these experiments. Outside of the ICF application, stopping power is a quantity which can be directly measured by experiment [6–12]. Since it is a result of ion-electron collisions, it is also a proxy for other transport properties determined by electron-ion collisions such as electrical and thermal conductivities. Thus, it is a good example property to test transport theory.

Here, a model is presented to calculate stopping power in the warm dense matter regime. The method applies the Boltzmann-Uehling-Uhlenbeck (BUU) [13, 14] equation, but treats ion-electron interactions with the potential of mean force rather than the Coulomb potential or screened Coulomb (Debye) potential [15–17]. With this combination, the degeneracy and strong correlation effects relevant to the warm dense matter regime are self-consistently accounted for. The resulting model may be viewed in two ways: as an extension of the theory of weakly coupled degenerate gases to the strongly coupled regime with the use of the potential of mean force, or as an extension of mean force kinetic theory [18, 19] into the degenerate regime by generalizing the kinetic equation from a Boltzmann operator to the BUU operator. Further, the approach introduced in Ref. [20] has been generalized to arbitrary velocities for the interacting particles, enabling the calculation of stopping power.

Warm dense matter is typically defined by a region of density and temperature parameter space where three dimensionless parameters merge; see Figure 1. The first is the Coulomb coupling parameter, defined by

$$\Gamma_{ss'} = \frac{q_s q_{s'}}{4\pi\epsilon_0 a k_B T}, \quad (1)$$

where q_s is the charge of species s , $a = (3/4\pi n)^{1/3}$ is the average interatomic spacing or the Wigner-Seitz radius, and T is the system temperature. This measures the ratio of the average potential energy of the system against the average thermal kinetic energy. Second, the degeneracy parameter is defined as

$$\Theta = \frac{k_B T}{E_F}, \quad (2)$$

where $E_F = \hbar^2(3\pi^2 n_e)^{2/3}/(2m_e)$ is the electronic Fermi energy and n_e is electron density. This parameter elucidates when the electron-electron interactions become dominantly quantum mechanical. Finally,

$$r_s = \frac{a}{a_0} = 1.8 \frac{q^2}{4\pi\epsilon_0 a E_F} \quad (3)$$

is defined as the Coulomb coupling parameter in the degenerate regime. Here, $a_0 = 4\pi\epsilon_0 \hbar^2/m_e e^2$ is the Bohr radius. Once $\Theta < 1$, the relevant kinetic energy of the system is no longer the thermal average and is replaced by the Fermi energy.

Warm dense matter occurs when all these parameters (Γ , Θ , and r_s) are of order unity. By definition then, it is impractical to develop a theory for warm dense matter which expands about any of these parameters. Classical plasma physics theories tend to follow two formalisms: binary scattering [21–24] and linear response [25]. These theories fall in the classical non-degenerate regime of figure 1, where $\Gamma \ll 1$ and $\Theta \gg 1$, and are not suited for warm dense matter. An alternative is to use classical molecular dynamics [26–28], where Newton’s equations

of motion are solved on a set of particles. In principle, this should be valid for all classical areas of figure 1 ($\Theta \gg 1$), but is computationally expensive. On the other end of the spectrum, condensed matter based theories are based on methods treating the strongly coupled degenerate regime of figure 1 where $\Gamma \gg 1$ and $\Theta \ll 1$. The leading technique in condensed matter is time-dependent density functional theory (TDDFT) [29–35], which attempts to solve the quantum N-body problem for a set of atoms and a projectile. In principle, TDDFT can simulate all conditions, but at low densities and high temperatures the number of quantum states necessary is so large that the problem becomes intractable. As such, the need for intermediate theories that attempt to bridge the gap between TDDFT and the traditional plasma physics regime is needed. Approaches of this type tend to extend plasma theories either through effective potentials in binary scattering theories [18, 19, 28, 36] or through the use of local field corrections and structure factors in linear response theory [28, 36, 37]. To include the quantum effect of diffraction in particle scattering, a quantum cross section can be considered in place of a classical one [38, 39]. Additionally, the stopping power resulting from an expression similar to these has been integrated over the course of a particle trajectory to calculate its net energy exchange with the plasma [7, 40]. Finally, the free electron gas can be considered in place of the ideal gas, and similar to the classical non-degenerate regime, both binary scattering [20, 41–43] and linear response [44–49] formalisms for the free electron gas have been developed.

The present theory is an extension of a Boltzmann kinetic equation, similar to traditional plasma kinetic theory, but which utilizes the mean force construct [18, 19] to extend it to stronger coupling, and the BUU equation to account for degeneracy in the particle statistics [13, 14, 20]. Electrons are treated as a Fermi gas, so they obey Fermi-Dirac statistics, and are treated with full quantum scattering. Additionally, the cross sections are computed based on the potential of mean force. This is the aspect that extends the model to strong coupling [18, 19]. Mean force kinetic theory [19] found that the potential of mean force is the correct interaction potential to preserve the exact equilibrium of a classical system. It is interaction force for a binary interaction that accounts for the presence of the other $N - 2$ particles in the system, treating them in the equilibrium limit. In this way, the static influence of many-body physics can be included in binary interactions. With the potential of mean force, Boltzmann’s molecular chaos approximation [50] can be relaxed, allowing the regime of plasma kinetic theory to be extended from $\Gamma \lesssim 0.1$ to $\Gamma \lesssim 30$ [18, 19].

The mean force method is then extended to quantum systems through the quantum potential of mean force defined in Ref. [17]. This method couples the typical Ornstein-Zernike equation to an average atom calculation [16] treating the electrons quantum mechanically. Along with quantum scattering and the inclusion of Fermi-Dirac statistics, the quantum potential of mean force extends

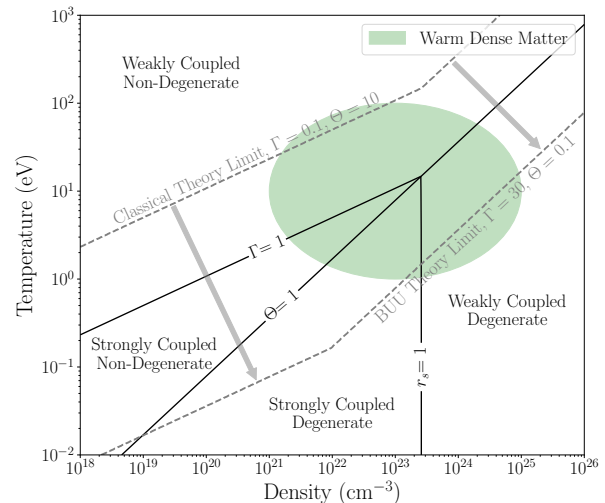


FIG. 1. The density temperature phase space around the warm dense matter regime denoted by the green shaded region. The phase space is split up by the lines $\Gamma = 1$, $\Theta = 1$, and $r_s = 1$, into four regions determined by the dominate energy in the system. The two dashed gray lines mark where classical plasma physics theories fail at $\Gamma = 0.1$ and $\Theta = 10$ and where the Boltzmann-Uehling-Uhlenbeck based theory extends this to at $\Gamma = 30$ and $\Theta = 0.1$.

the range of applicability of the theory from $\Theta \gtrsim 10$ to $\Theta \gtrsim 0.1$ [51]. The inclusion of these aspects of quantum physics allows the method to bridge the gap between traditional plasma and solid state regimes. Specifically, in the limit $\Theta \gg 1$, it is shown that classical plasma physics results are recovered. In the opposite limit $\Theta \ll 1$, results of the zero temperature Fermi gas are recovered.

These ideas have been explored previously with the quantum Landau-Fokker-Plank equation [43], which takes a small scattering angle approximation. Since this is motivated by a weak coupling approximation, it makes the application of theory to higher coupling unclear. The present theory uses a Boltzmann type operator that includes all strengths of scattering. The crossover from classical to Fermi liquid behavior was also explored by Daligault [52] through a calculation of the momentum lifetime of an electron, showing the transition from the weakly coupled classical plasma limit where the Coulomb logarithm arises, to the Fermi degenerate limit where the scaling laws of Fermi liquid theory are returned. A similar transition is observed here based on an electron-ion collision rate obtained from the low-speed limit of the stopping power.

In ICF modeling, stopping power is an input to large and computationally expensive hydrodynamic simulations. Commonly, an analytic formula best suited for the classical weakly coupled regime is used [21, 23, 24]. This is due to the ease of calculation, as these theories have a closed form solution and can be evaluated nearly instantaneously during the simulation. However, past the classical theory limit shown in figure 1, the approxima-

tions within these expressions begin to fail in an uncontrolled way. This can, for example, lead to unphysical predictions such as negative collision frequencies. Alternatively, tabulated values from TDDFT simulations can be used as input, but these calculations tend to be extremely computationally expensive [35] at the relatively high temperatures characteristic of warm dense matter. This causes these simulations to take on the order of days to complete, which limits their practicality for exploring the broad range of material conditions relevant to ICF. The approach presented here, while an extension of the classical weakly coupled theories, contains controlled approximations valid in the warm dense matter regime. The cost of this is a larger computation time when compared to the analytic theories, but still far less than TDDFT. Thus, tables of stopping powers for a large array of densities, temperatures, and projectile energies can be computed using the present method in a fraction of the time it would take for a method based on TDDFT.

The paper is outlined as follows. In section II, the kinetic theory is outlined and an expression for the stopping power is derived. In section III, the expression is evaluated and compared to other leading theories. Next, section IV examines the asymptotic limits of the stopping power and the transition between classical and degenerate behavior is discussed. Finally, in section V, the Barkas effect [53] in degenerate plasmas is commented on.

II. THEORY

A. Boltzmann-Uehling-Uhlenbeck Equation

The BUU equation is a semi-classical generalization of the classical Boltzmann equation. Its collision term is given by [13]

$$C_{ss'} = \int d^3p_{s'} d\Omega \frac{d\sigma}{d\Omega} u \left[\hat{f}_s \hat{f}_{s'} (1 + \delta_s \theta_s f_s) (1 + \delta_{s'} \theta_{s'} f_{s'}) - f_s f_{s'} (1 + \delta_s \theta_s \hat{f}_s) (1 + \delta_{s'} \theta_{s'} \hat{f}_{s'}) \right], \quad (4)$$

where $u = |\mathbf{p}_s/m_s - \mathbf{p}_{s'}/m_{s'}|$ is the relative speed of the collision, $d\sigma/d\Omega$ is the differential scattering cross section, $\theta_s = (2\pi\hbar)^3/g_s$ is the phase space volume occupied by each electron, g_s is the spin multiplicity of the species s , and $\delta_s = -1, 0, 1$ for Fermi-Dirac, Maxwell-Boltzmann, and Bose-Einstein statistics respectively for species s . As in the classical Boltzmann equation, hatted quantities denote they are taken post collision, and unhatted quantities are taken before a collision. In this work, the differential scattering cross section, $d\sigma/d\Omega$, is determined using the potential of mean force which will be defined in section II B.

This collision operator describes the evolution of the Wigner function, which is a generalization of the classical velocity distribution function and a representation of the density matrix of quantum statistical mechanics [54].

Overall, the BUU collision operator can be derived from the Heisenberg equation of motion for a quantum system in an analogous way to how the classical Boltzmann equation is derived from the Liouville equation [55]. This includes an approximation similar to molecular chaos, which amounts to weak coupling. This means the BUU operator inherits a binary scattering approximation in which only two-body interactions are explicitly solved for. The equilibrium state of the BUU collision operator can be shown to be the Fermi-Dirac or Bose-Einstein distribution. Since only electrons will be treated quantum mechanically here, and are fermions, the Fermi-Dirac distribution will be used. This is defined as

$$f_s(\mathbf{p}) = \frac{1}{\theta_s} \frac{1}{\exp(\frac{\beta(\mathbf{p} - m_s \mathbf{V}_s)^2}{2m_s} - \beta\mu_s) + 1}, \quad (5)$$

where \mathbf{V}_s is the flow shift of species s with respect to an inertial reference frame, $\beta = 1/(k_B T)$ is the inverse temperature, and μ_s is the chemical potential of species s . The chemical potential is uniquely determined by the normalization condition $\int d^3p f_s(\mathbf{p}) = n_s$, which implies

$$\mathcal{Q}_{1/2}(\beta\mu) = \frac{4}{3\sqrt{\pi}} \Theta^{-3/2}, \quad (6)$$

where $\mathcal{Q}_{1/2}(z)$ is a Fermi-Dirac integral of order 1/2. The Fermi-Dirac integral of arbitrary order is defined as

$$\mathcal{Q}_j(x) = \frac{1}{\Gamma(j+1)} \int_0^\infty \frac{y^j}{e^{y-x} + 1} dy, \quad (7)$$

where $\Gamma(x)$ is the gamma function.

The most glaring difference between Eq. (4) and the classical Boltzmann equation are factors in the form of $(1 + \delta\theta f)$. In the case of electrons, or any fermion, these are Pauli-blocking terms. When a fermion undergoes a binary collision, the final state of the fermion after the collision cannot be occupied. Thus, the term $(1 + \delta\theta \hat{f})$ tracks the available states a particle can occupy once the collision has completed. Classically, $\delta = 0$ and this effect disappears, as all states are equally probable.

The final difference to note between Eq. (4) and the classical Boltzmann equation is the evaluation of the differential scattering cross section. Since scattering in warm dense matter is not always classical, a quantum description of scattering is used. The scheme used is based on the procedure outlined in Ref. [56]. Since the model is based on a binary interaction assumption, Pauli-blocking does not influence the calculation of the cross section. It is accounted for by the weighting factors $(1 + \delta\theta f)$ described above. Details of this calculation are given in Appendix A.

B. Potential of Mean Force

The major result of classical mean force kinetic theory [18, 19] is that collective interactions in a plasma

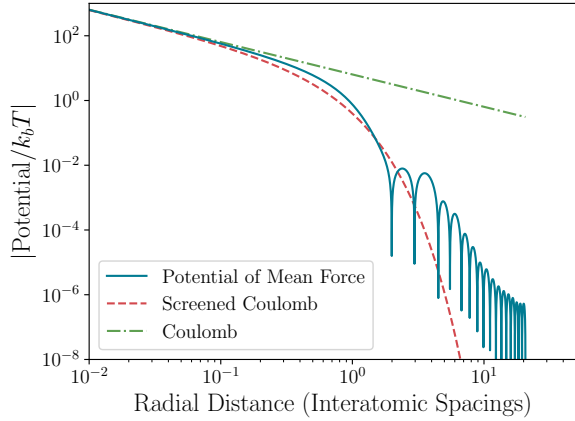


FIG. 2. Scattering potentials for hydrogen at 5eV and 1.67 g/cc. This translates to $\Gamma = 4.65$ and $\Theta = 0.14$, putting this example firmly in the warm dense matter regime. The blue line is the potential of mean force calculated from the average-atom two-component plasma model [16, 17]. The red dashed line is a screened Coulomb potential with a screening length determined by a combination of the Debye length and the Thomas-Fermi length [57]. The green dashed line shows the Coulomb potential. Notice how the potential of mean force contains screening absent from the Coulomb potential, and the correlation effects absent from the other potentials.

can be modeled using an effective potential in the kinetic equation. The correct potential for a classical system has been rigorously shown to be the potential of mean force [19]. Formally, the potential of mean force is the force between 2 particles held at fixed positions obtained by averaging over the remaining $N - 2$ particles in thermodynamic equilibrium. It is often calculated using the Ornstein-Zernike equation along with a corresponding closure equation [15]. For Coulombic systems, the hyper-netted chain approximation is often an accurate closure, which results from the assumption that the difference between direct and indirect correlations are sufficiently small [15]. In quantum statistical mechanics, an analogous averaging procedure can be done [54], but the factoring of positions and momenta necessary to fix the positions of two particles cannot be done. Thus, a quantum analog to Ref. [19] has not been attempted.

In warm dense matter, ions can still be treated classically [51]. Due to this, the potential of mean force can be defined for ion-ion interactions including screening from degenerate electrons using the average-atom two component plasma model [16]. The idea is that the electronic structure of the ions needs to be described using an average atom (or atom in jellium) model to properly classify electrons as bound or free. Once this is done, the ions can be coupled together using the Ornstein-Zernike equation and a quantum hypernetted chain closure, which includes the additional screening degenerate electrons provide between the ions. This was further ex-

tended to model free electrons interacting with these average atoms [17]. The definition used here is (given in atomic units $\hbar = m_e = a_0 = e = 4\pi\epsilon_0 = 1$) from Ref. [17]

$$V_{ie}^{\text{MF}}(r) = -\frac{Z}{r} + \int d^3r' \frac{n_e^{\text{ion}}(r')}{|\mathbf{r} - \mathbf{r}'|} + V^{\text{XC}}[n_e^{\text{ion}}(r)] \\ + n_i^0 \int d^3r' \frac{C_{ii}(|\mathbf{r} - \mathbf{r}'|)}{-\beta} h_{ii}(\mathbf{r}') \\ + \bar{n}_e^0 \int d^3r' \frac{C_{ie}(|\mathbf{r} - \mathbf{r}'|)}{-\beta} h_{ie}(\mathbf{r}'), \quad (8)$$

where Z is the atomic number of the ionic species, n_e^{ion} is the density of bound atoms around an average atom, n_i^0 is the number density of ions in the plasma, \bar{n}_e^0 is the average density of free electrons in the plasma, C_{ii} and C_{ie} are the direct correlation functions for ion-ion and ion-electron interactions, h_{ii} and h_{ie} are ion-ion and ion-electron pair correlation functions, and V^{XC} is the exchange correlation potential. The choice of V^{XC} is determined by the system in question. Here, the Dirac exchange potential [58] (local density approximation) is used.

All quantities in Eq. (8) are determined self-consistently through the average atom two component plasma model [16]. It is important to note that within the average atom two component plasma model, the average ionization \bar{Z} is determined by the spatial integral over the free electron density, defined as the electrons with positive energy. Within the model, the point of zero energy is self-consistently determined. Thus, any continuum lowering due to strong correlations is included in the free electron density. In this manner, the ionization, and thus electron density, can be a non-integer value, which is not physical for a single isolated ion. However since the model solves for the average atom of a system, this is a good approximation of the mean ionization [59].

Overall, the potential of mean force includes multi-particle correlations which are not present in most scattering potentials. The correlations manifest in oscillations and correspond to average particle positions in the plasma. This can be seen in Fig. 2, which shows various choices for scattering potentials in hydrogen at 1.67g/cc and 5eV. These density and temperature conditions translate to Coulomb coupling strength of $\Gamma = 4.65$ and a degeneracy parameter of $\Theta = 0.14$ corresponding to the warm dense matter regime. This is why mean force kinetic theory, and hence the present theory, can extend to higher coupling. It is due to the additional screening and correlations that the potential of mean force captures.

C. Stopping Power

With these ideas, an expression for stopping power can be developed. Following Ref. [20], the stopping power is computed from the friction force density between two

species in the plasma

$$\mathbf{R}_{ss'} = \int d^3p_s \mathbf{p}_s \mathcal{C}_{ss'}. \quad (9)$$

As with classical collisional processes, the largest momentum transfer occurs between particles of similar average speeds. In an equilibrium plasma the ratio between the speed of ions and the speed of electrons is $v_{av,e}/v_{av,i} \approx \sqrt{m_i/m_e} \sim 43$, at the least, due to their relative mass difference. In ICF, fusion alpha particles are born at 3.5 MeV [60]. This means that thermal electrons provide the largest momentum transfer, and hence stopping power, at a thermal energy of around 1 keV. If instead the alpha particles were to stop on thermal protons, the maximal momentum transfer would require the protons to have a thermal energy of 100s keV. As such, the only contribution considered here is of ballistic ions stopping on free electrons. The projectile ion species s' is approximated as a beam with velocity \mathbf{V}_i . As such, its velocity distribution function is given by $f_i(\mathbf{p}) = n_i \delta(\mathbf{p} - m_i \mathbf{V}_i)$, where n_i is the density of ballistic ions, and δ is the Dirac delta function. The free electrons follow the Fermi-Dirac distribution given in Eq. (5), and have a free electron density n_e determined by the average ionization, \bar{Z} , from the average atom two component plasma model.

Additionally, two simplifications can be made to the integrals of Eq. (9). The first takes advantage of the mass ratio already used to isolate electronic stopping power. When an electron and ion undergo a binary collision, the change in velocity of the ion is much smaller than that of the electron. This means it is a good approximation to take the limit $m_r = m_e/m_i \ll 1$ in order to simplify the collision physics. Since the integrals and distribution functions were defined in terms of momenta above, which includes a factor of the mass, these are changed to velocities here. Along with this, it is helpful to normalize all velocities by the electron thermal speed, from this point forward $\tilde{\mathbf{v}}_s = \mathbf{v}_s/v_{te}$ and $\tilde{\mathbf{V}}_s = \mathbf{V}_s/v_{te}$, where $v_{te} = \sqrt{2k_B T/m_e}$. The second simplification takes ad-

vantage of symmetries present in the differential scattering cross section. It is known that the scattering cross section should be symmetric with respect to time reversal and space inversion [61]. This means that the pre and post collision velocities in the collision operator can be exchanged and the expression will still hold. This is a manifestation of the principle of detailed balance for a binary, elastic collision [50, 62–64].

Using these simplifications, Eq. (9) becomes

$$\mathbf{R}_{ie} = -\frac{m_e n_i n_e v_{te}^2}{Q_{1/2}(\beta\mu_e)\pi^{3/2}} \int d^3\tilde{\mathbf{u}} d\Omega \frac{d\sigma}{d\Omega} \frac{\tilde{\mathbf{u}} \Delta \tilde{\mathbf{u}}}{e^{(\tilde{\mathbf{u}} + \Delta \tilde{\mathbf{V}})^2 - \beta\mu_e} + 1} \times \left[\frac{e^{(\tilde{\mathbf{u}} + \Delta \tilde{\mathbf{u}} + \Delta \tilde{\mathbf{V}})^2 - \beta\mu_e}}{e^{(\tilde{\mathbf{u}} + \Delta \tilde{\mathbf{u}} + \Delta \tilde{\mathbf{V}})^2 - \beta\mu_e} + 1} \right], \quad (10)$$

where $\Delta \tilde{\mathbf{u}} = (\hat{\mathbf{u}} - \mathbf{u})/v_{te}$ is the change in the relative velocity vector \mathbf{u} , and $\Delta \tilde{\mathbf{V}} = \tilde{\mathbf{V}}_i - \tilde{\mathbf{V}}_e$ is the velocity of the ballistic ions in the center of mass reference frame of the electrons. The expressions of Ref. [20] can be obtained by taking the limit $|\Delta \tilde{\mathbf{V}}| \ll 1$ in Eq. (10). Stopping power is a drag force, which is obtained from the friction force density as \mathbf{R}_{ie}/n_i . Since it acts antiparallel to the ion velocity vector, the relationship between \mathbf{R}_{ie} and stopping power is given by

$$-\frac{dE}{dx} = \frac{\Delta \mathbf{V}}{\Delta V} \cdot \frac{\mathbf{R}_{ie}}{n_i}, \quad (11)$$

where dE/dx is the stopping power.

It is clear that Eq. (10) must be evaluated numerically. However, further simplifications can be made. First the integral is put into spherical coordinates and a reference frame is chosen such that the only free parameter, $\Delta \mathbf{V}$, is oriented along the cartesian z-axis. Details of the explicit vector components are given in Appendix B. Once the transformation into this reference frame is substituted into Eq. (10), it is then a simple math exercise to reduce the expression into the form

$$\mathbf{R}_{ie} = \frac{2m_e n_i n_e v_{te}^2}{Q_{1/2}(\beta\mu_e)\pi^{1/2}} \frac{\Delta \tilde{\mathbf{V}}}{\Delta \tilde{V}} \int d\tilde{u} d\theta' d\theta d\tilde{\phi} \sin\theta' \sin\theta \frac{d\sigma}{d\Omega} \tilde{u}^4 \frac{(1 - \cos\theta) \cos\theta' + \sin\theta' \sin\theta \cos\tilde{\phi}}{e^{\tilde{u}^2 + \Delta \tilde{V}^2 + 2u\Delta \tilde{V} \cos\theta' - \beta\mu_e} + 1} \times \left(1 - \frac{1}{e^{\tilde{u}^2 + \Delta \tilde{V}^2 + 2u\Delta \tilde{V} g(\theta, \theta', \tilde{\phi}) - \beta\mu_e} + 1} \right), \quad (12)$$

where θ' is the polar angle for the spherical integration of $\tilde{\mathbf{u}}$, θ is the polar scattering angle, $\tilde{\phi} = \phi - \phi'$, where ϕ' and ϕ are the azimuthal angles for the integration of $\tilde{\mathbf{u}}$ and the scattering angle respectively. Finally $g(\theta, \theta', \tilde{\phi}) = \cos\theta \cos\theta' - \sin\theta \sin\theta' \cos\tilde{\phi}$ is an angular factor describing the angle between $\Delta \tilde{\mathbf{u}}$ and $\Delta \tilde{\mathbf{V}}$.

In comparison to Eq. (10), Eq. (12) is simpler to evaluate because it is a 4-dimensional rather than 5-dimensional integral, and only one of the integrals is improper. Despite this, the integral does display some challenges since the distribution functions depend explicitly on all angular integration variables. This means this

integral cannot be separated any further and the differential scattering cross section cannot be reduced into a momentum transfer or energy transfer cross section.

It is important to state that due to the use of the average atom model, only unbound electrons are taken to participate in the stopping. This is reasonable if the system in question has pressure ionized all but a few core electrons, or if the system is not dense at all. This makes various forms of hydrogen and lower Z elements good candidates for this theory. Additionally, since the atomic structure is not being explicitly solved for, inelastic processes such as bound-free transitions are not solved for.

III. RESULTS

As a test case, we consider deuterons stopping in warm dense deuterium. This was chosen because it is relevant to ICF implosions [65], and because there is previous calculation data to compare with. Specifically, the results are compared to two analytic theories [23, 24] from the classical weakly coupled region of Fig. 1, and two formalisms of TDDFT molecular dynamics simulations [32]. Time dependent density functional theory is a quantum mechanical technique to simulate many body quantum systems. In the results compared against, electronic wave functions were time evolved in two different ways. The Kohn-Sham formalism solves for wave functions using a time-dependent extension to the Kohn-Sham equation [66, 67] along with the Mermin extension for finite temperature [68]. As such, TDDFT carries similar assumptions and approximations as finite temperature time-independent DFT, for example the exchange-correlation potential or the initial distribution of occupied states. Since the comparison is done with a simple element, deuterium, it is expected that Kohn-Sham TDDFT should be a good approximation to the system, as it has been used in many other warm dense matter systems [34, 35, 69]. This makes it a good benchmark for the present theory. One additional drawback of TDDFT is that it is extremely computationally expensive, often requiring extreme computational resources [34, 35]. It has been shown to scale as the cube of temperature [32], making convergence in the temperature regimes of warm dense matter difficult.

Figure 3 shows that for the cases chosen, the BUU theory matches the Kohn-Sham TDDFT fairly well, with the largest deviations occurring near the Bragg peak. They agree especially well at low projectile speeds where the stopping power can be related to linear transport process such as electrical conductivity. Agreement between these two methods in this regime has been shown before [20]. The surprising agreement comes at higher velocities. At high projectile speeds, it is standard to use velocity dependent potentials, known as dynamic screening, to capture the linear response of the plasma to the projectile [37, 46, 47]. Time dependent density functional theory can self consistently solve for this, but the potential

of mean force is a static, velocity-independent potential which means that dynamic aspects of the linear response are not included. The agreement may be due to the fact that in the present theory, collisions with electrons are treated fully quantum mechanically. This includes the full treatment of quantum scattering in the partial wave expansion, and the inclusion of Pauli blocking in the collision operator to properly weight collisions.

At projectile speeds around the Bragg peak, the model shows the largest disagreement with the Kohn-Sham TDDFT. This is also where the different TDDFT methods have the largest scatter in the data, and where they disagree with one another most. In Ref. [32], the scatter in the data was largely attributed to finite size effects in the simulation. It was also mentioned that the TDDFT data includes effects of bound electrons in the projectile particle and that better agreement with dielectric-function based models was achieved if the projectile is fully stripped. A similar effect may be of some influence here, as any inelastic physics of bound-free transitions, which result from dynamic many body effects, can be modeled by TDDFT, but are absent from the present theory.

A comparison is also made to orbital free TDDFT. In this formalism, electrons are treated semi-classically with a finite temperature Thomas-Fermi type equation [32, 70]. This is not expected to capture bound electron physics, but is a good approximation at higher temperatures where warm dense matter exists. Its scaling in temperature is not as severe as the Kohn-Sham variety, but it still relies on molecular dynamics which is computationally expensive on its own [32]. As such, the orbital free density functional theory is consistent with the Kohn-Sham variety and the present method away from the Bragg peak, but disagrees at the Bragg peak.

Finally, two analytic models which are commonly used in ICF applications are compared to. These are the Li-Petrasso [23] and Brown-Preston-Singleton [24] theories. They are both formulated using a Fokker-Plank type equation along with the Coulomb potential, which is not valid at strong coupling and hence warm dense matter. In both, a correction is included which is attributed to plasma screening. This is a step towards including dynamic screening, which could explain the difference in the predicted tail of these two theories when compared to either of the TDDFT methods or the BUU method. The more likely cause of the disagreement is the Coulomb coupling. All of the cases considered in Fig. 3 have a Coulomb coupling parameter $\Gamma > 0.4$. These plasmas are too strongly coupled for these analytic theories which explicitly expand about $\Gamma \ll 1$ [23, 24]. Additionally, Li-Petrasso and Brown-Preston-Singleton do not contain any notion of Pauli blocking. Pauli blocking limits the energies electrons can leave a collision with, which means that collisions which these models predict energy transfer from the projectile to the plasma could actually be blocked. This would lead to an overall reduction in the stopping power, which is observed.

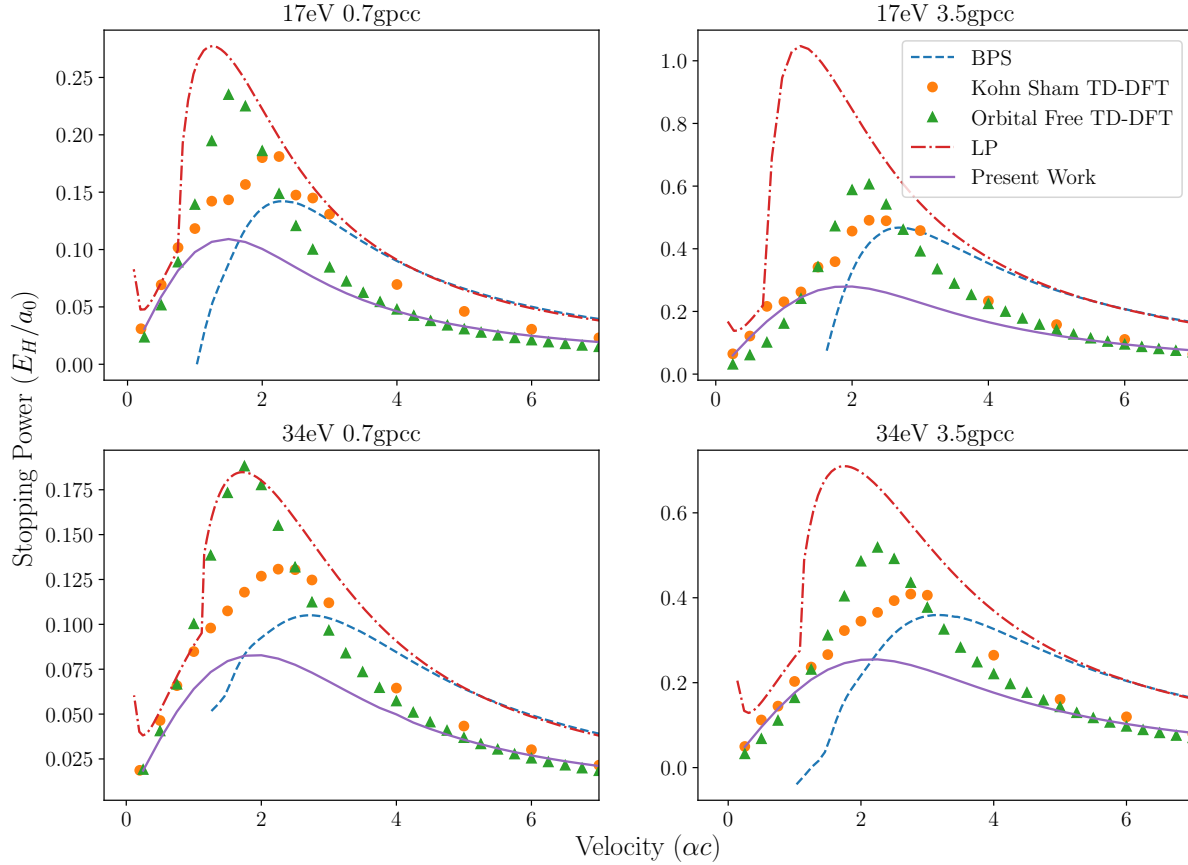


FIG. 3. Stopping power of a deuteron in warm dense deuterium at various densities and temperatures. The results of the present method are shown as solid purple lines. This is compared to two analytic theories: Brown-Preston-Singleton [24] (dashed blue lines) and Li-Petrasso [23] (dashed-dotted red lines). We also compare to orbital-free (green triangles) and Kohn-Sham (orange circles) TDDFT calculations [32]. Our method matches the density functional theory calculations in both the low speed and high speed limits. Neither analytic theory is consistent with both the high and low velocity limits of the density functional theory, as they are not well suited for the warm dense matter regime. Units are given in atomic units where $E_H = 27.2\text{eV}$ is the Hartree energy, a_0 is the Bohr radius, and $\alpha = e^2/(4\pi\epsilon_0\hbar c)$ is the fine structure constant.

The main benefit of the BUU approach is that it can capture the relevant strong coupling and quantum effects relevant to warm dense matter at a fraction of the computational cost. Especially at lower speeds, away from velocities which require the need of dynamic screening or inclusion of bound-free electron transitions. With this in mind, it is expected this approach should work best when there are few bound electrons in the plasma or when the bound electrons are highly localized around their nucleus.

Additionally, predictions were made for the stopping of protons in hydrogen at 1.67 g/cc at temperatures ranging from 0.5 eV to 1 keV; see Figure 4. A predicted consequence of the Pauli blocking factors in the BUU equation is that the stopping power curve is insensitive to temperature when $\Theta \ll 1$. This is because collisions are limited to an energy range of width $k_B T$ around the Fermi energy. When the temperature becomes small, this energy range collapses so that collisions can only occur at the Fermi energy. The Fermi energy is temperature independent, so stopping power should not have explicit

temperature dependence in this limit. This expectation is born out in the data shown in Fig. 4(a), which shows the stopping powers for a range of temperatures in the degenerate regime ($\Theta < 1$). In contrast, the stopping power curve in the classical regime ($\Theta > 1$) depends strongly on temperature. Here there is no blocking of states, and electrons can scatter across the full thermal distribution of energies. A consequence is that the Bragg peak will follow the average speed of thermal distribution, the thermal speed. This can be seen in Fig. 4(b) which shows stopping powers for a range of temperatures in the classical regime.

This behavior signifies there is a transition across the warm dense matter regime from classical plasma physics to degenerate plasma physics [52]. This transition is the illustration of why Θ is the proper parameter to characterize the degeneracy of the system. It signifies when the system transitions from being determined by the thermal energy $k_B T$ to the Fermi energy [71]. This phenomenon has even been observed in experiments on the National

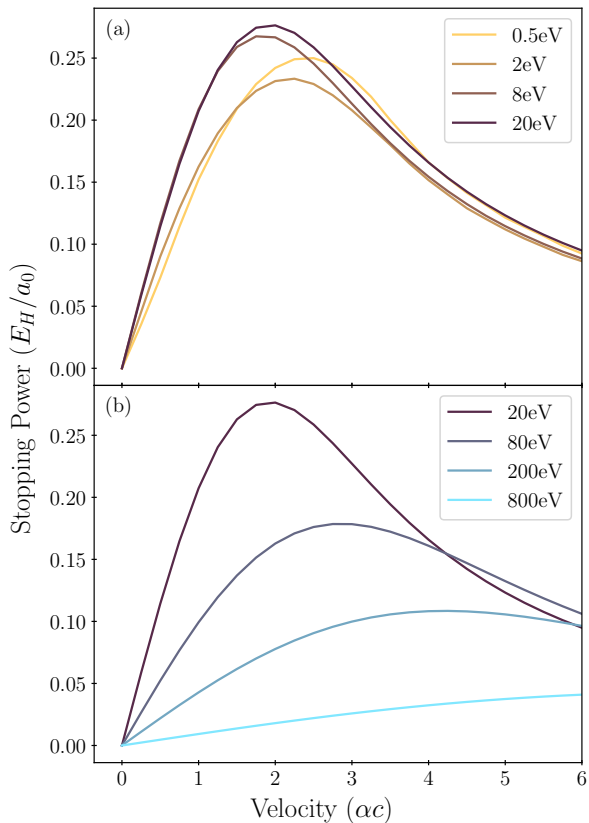


FIG. 4. Predictions of proton stopping power in hydrogen at 1.67 g/cc and various temperatures. Panel (a) shows the results from 0.5eV to 20eV, which are characterized by a degenerate regime, $\Theta < 1$. Panel (b) shows the results for 20eV to 800eV, which are characterized by a classical regime, $\Theta > 1$. Notice that the stopping power curves for the degenerate cases in (a) do not change very much over the span of temperatures. This is because the ballistic proton is stopping on electrons at the Fermi energy, which is temperature independent. Whereas in (b), the curve changes substantially with temperature as the proton is stopping on electrons at the thermal velocity, which increases with temperature. Units are given in atomic units where $E_H = 27.2\text{eV}$ is the Hartree energy, a_0 is the Bohr radius, and α is the fine structure constant.

Ignition Facility [10] and the Omega laser [72].

IV. ASYMPTOTIC BEHAVIOR OF STOPPING POWER IN WARM DENSE MATTER

Along with the stopping power, the electron-ion collision frequency is expected to display different scalings with respect to density and temperature in the classical and degenerate regimes. Again, this is because collisions in the classical regime sample the entire temperature range of the Maxwell-Boltzmann distribution, whereas in the degenerate regime Pauli blocking limits them to around the Fermi energy. This fundamentally changes

how energy and momentum are transported in degenerate as opposed to classical plasmas [52].

From the stopping power, the electron-ion collision frequency can be found by taking the small projectile velocity limit. Explicitly this is done by taking the limit $\Delta\tilde{V} \ll 1$ in Eq. (12), which yields

$$R_{ie} = -m_e n_e \nu_{ei} \Delta V, \quad (13)$$

where

$$\nu_{ei} = \frac{8}{3} \frac{n_i v_{te}}{\mathcal{Q}_{1/2}(\beta\mu_e) \pi^{1/2}} \int_0^\infty d\tilde{u} \sigma_p \tilde{u}^4 G(\tilde{u}^2), \quad (14)$$

is the electron-ion collision frequency, σ_p is the momentum transfer cross section defined as

$$\sigma_p = \int d\Omega \frac{d\sigma}{d\Omega} (1 - \cos \theta), \quad (15)$$

$G(\epsilon)$ is related to the availability of states given by

$$G(\epsilon) = \frac{\sqrt{\epsilon} e^{\epsilon - \beta\mu_e}}{(e^{\epsilon - \beta\mu_e} + 1)^2} = \sqrt{\epsilon} f_{\text{FD}}(1 - f_{\text{FD}}), \quad (16)$$

where f_{FD} is the Fermi-Dirac distribution, and $\epsilon = \tilde{u}^2$ is the dimensionless relative particle energy. In comparison to Eq. (12), Eq. (13) is much simpler to evaluate as all but one integral can be integrated out or absorbed into other factors. The momentum transfer cross section has a much simpler form than the differential scattering cross section due to angular symmetries. This is shown for quantum scattering in Appendix A.

When changing the temperature (at a constant density of 1.67 g/cc) and changing the density (at a constant temperature of 20 eV) while evaluating Eq. (13), different behavior exists in the degenerate and classical regimes. This can be seen in Fig. 5, but to make this more evident, explicit expansions in large and small Θ can be performed.

In the classical limit $\Theta \gg 1$, the availability of states $G(\epsilon)$ reduces to a Maxwellian form, and the classical result is recovered [21]

$$\nu_{ei}^C = \frac{8}{3} \frac{n_i v_{te}}{\pi^{1/2}} \int_0^\infty d\tilde{u} \sigma_p \tilde{u}^5 e^{-\tilde{u}^2}. \quad (17)$$

The results from this expression, Eq. (17), follow the scalings in temperature and density of $\nu_{ei}^C \sim T^{-3/2} \ln(T)$ and $\nu_{ei}^C \sim -\ln(n_e)$ respectively. This is the expected picture from the view of classical plasma physics [21].

In the degenerate limit, $\Theta \ll 1$, it is not clear how to expand $G(\epsilon)$ with a simple Taylor expansion. Thus, it is informative to examine the behavior of $G(\epsilon)$ as a function of Θ . In this regime, Pauli blocking prevents electrons far from the Fermi energy from participating in collisions. This means $G(\epsilon)$ can be approximated as a Dirac delta function around the Fermi energy to a good approximation as $\Theta \rightarrow 0$. This behavior is illustrated in Fig. 6 for four different values of Θ . Interestingly, this

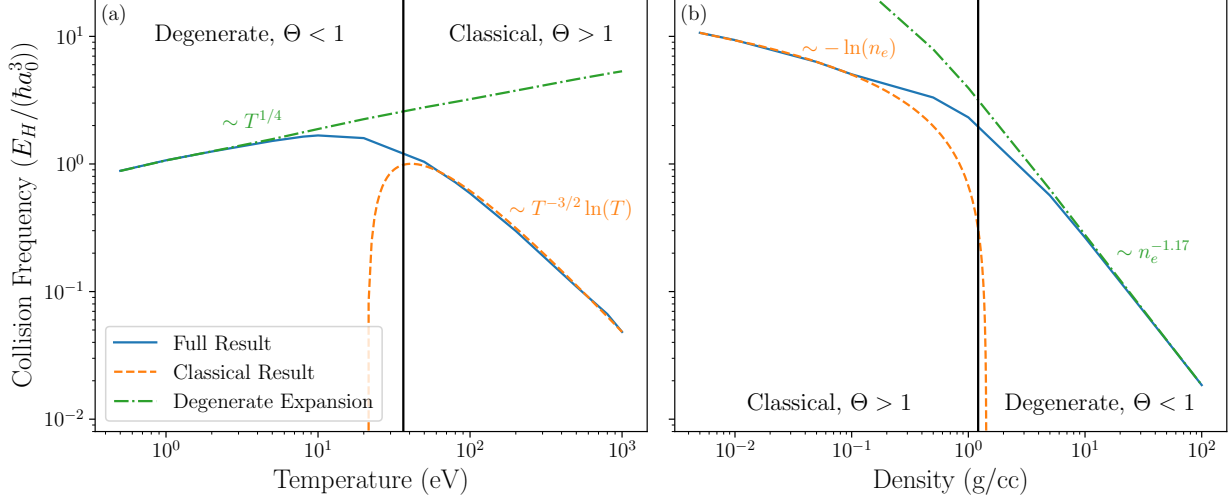


FIG. 5. Electron ion collision frequency of a hydrogen plasma computed using Eq. (14). The two plots show the (a) temperature and (b) density dependence in both the degenerate and classical limits. Notice that the behavior of the two limits is qualitatively very different, suggesting that the characteristic energies involved in collisions has changed from the thermal speed of the plasma to the Fermi energy. The black vertical line on both plots denotes the point $\Theta = 1$, and represents the location of the transition, as well as where warm dense matter conditions are present. Units are given in atomic units where $E_H = 27.2\text{eV}$ is the Hartree energy, a_0 is the Bohr radius, and α is the fine structure constant. Note that the collision frequency calculated is actually divided by the ion density, n_i , as a density of ions for a ballistic projectile has no physical meaning.

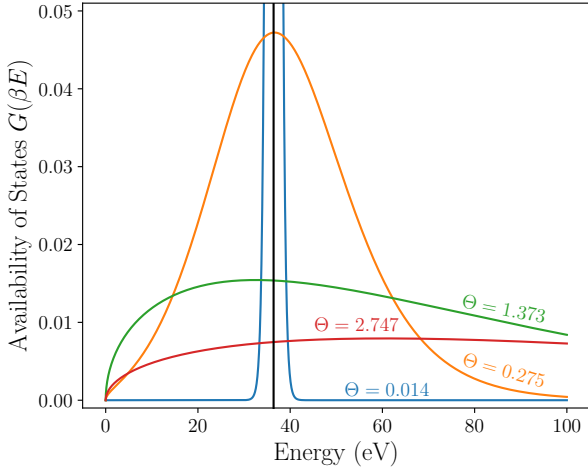


FIG. 6. The availability of states given by Eq. (16) is plotted for various values of Θ . Here β is the inverse temperature and E is the energy in electron volts. This function can be thought of as related to the occupancy of states in the plasma. Notice that when $\Theta > 1$, we seem to recover an exponential trend, similar to a Maxwell-Boltzmann distribution. When $\Theta < 1$, the distribution follows a peaked form and begins to become strongly peaked around the Fermi energy denoted by the black vertical line. This suggests that electrons are only able to undergo a collision if they sit around the Fermi energy.

argument is not dissimilar from those commonly made of continuum electrons in metals [73]. In fact, this is the motivation for the Sommerfeld expansion [74]. The

expansion involves assuming the distribution function is strongly peaked around a point, which Fig. 6 shows to be the Fermi energy. Then, a Taylor expansion of the remaining part of the integrand around that point is taken. For this case, the rest of the integrand includes the cross section, which is not known analytically and is therefore difficult to expand. Alternatively, the lowest order term can be obtained by taking the availability of states $G(\epsilon)$ to be a Dirac delta function around the Fermi energy. Doing so leaves the expression

$$\nu_{ei}^Q = n_i \sqrt{\frac{2E_F}{m_e}} \sigma_p(E_F) \quad (18)$$

where $\sigma_p(E_F)$ is the momentum transfer cross section evaluated at the Fermi energy.

A weak temperature scaling is expected in Eq. (18). Although there is no explicit temperature dependence, the potential of mean force implicitly depends on temperature and is highly dependent on the material of interest. If a Coulomb potential were to be used, the expression would be completely independent of temperature. This result is fundamentally different than the classical scaling in both density and temperature, signifying a difference in physics due to the protons colliding with thermal electrons in the classical limit versus at the Fermi energy in the degenerate limit. Examining these expressions closer, notice $\nu_{ei}^C \propto v_t$, whereas $\nu_{ei}^Q \propto v_F$, where $v_F = \sqrt{2E_F/m_e}$ is the Fermi speed. These are the average speeds of a classical and degenerate gas respectively, further signifying how the statistics influences the speed at which particles can scatter, and in turn, the characteristic scaling of the

collision frequency. This is seen in Fig. 5, as the scalings in both density and temperature are different in the classical and degenerate regimes.

This same behavior can be translated to stopping power, which is why Fig. 4(b) can be described by classical plasma physics behaviors, whereas Fig. 4(a) is dominated by collisions at the Fermi energy. This is interesting because the presented theory is in principle a high temperature gas theory, but has qualitative similarities with some solid-state theories at lower temperatures. The overall accuracy of the calculations is questionable outside of the warm dense matter regime, since it is not expected that the necessary correlations are captured. Despite this, it is interesting to see the qualitative trends which seem to match scaling laws of Fermi liquids.

V. COMMENT ON THE BARKAS EFFECT

In classical plasma physics, collisional transport properties, including stopping power are symmetric about the sign of the charge. That is, an attractive interaction would have the same stopping power as a repulsive one does. It is the Coulomb potential specifically, which causes this symmetry as the Rutherford scattering cross section depends only on the square of the charges of the interacting particles. The potential of mean force is not Coulombic and is screened, thus this symmetry does not exist and results in the Barkas effect [53]. This means that the collision rate of an attractive interaction differs from that of a repulsive interaction. This has been studied before in classical strongly coupled plasmas [75] as well as strongly magnetized plasmas [76]. Since this work uses the potential of mean force, the Barkas effect is expected to be seen. This is an effect that the analytic and linear response theories do not capture as they either assume the force to be Coulombic or have a term proportional to the square of the charge, which is the manifestation of this symmetry.

VI. CONCLUSION

A model is presented for the stopping of ions in warm dense matter based on a combination of the BUU equation, which is a semi-classical generalization of the classical Boltzmann equation, and the mean force theory, which extends the model to strongly correlated conditions. This work serves as a generalization of Ref. [20] to arbitrary ion speeds. The model is compared to known theories of stopping power and shown to agree with state of the art TDDFT molecular dynamics simulations [32].

The result is a computationally efficient model that can be used to create tables of stopping powers for conditions ranging from weakly coupled classical plasmas to the warm dense matter regime. These could be used as inputs to hydrodynamic simulations relevant to ICF to improve the predictive power of the simulations. Addi-

tionally, the agreement with TDDFT in the tail of the stopping power curve implies that this work can be used to model experimental studies on stopping power, which tend to operate in the high speed tail.

The model was shown to capture the transition between between classical plasma physics to degenerate plasma physics qualitatively. This transition is described by the point $\Theta = 1$, where most of the electron scattering occurs at energies comparable with the Fermi energy instead of the average thermal energy. At this point, the ion-electron collision rate is weakly dependent on temperature, yielding a stopping power curve which does not appreciably change as Θ is further decreased. Qualitatively, this behavior is similar to that observed in solid state theories, which are often based on an ideal Fermi gas approximation.

Overall, the result is a natural extension of previous works in mean force kinetic theory [18–20] extending it further into the degenerate regime. Extensions would involve providing a systematic expansion of the BUU collision operator to provide a framework for calculating all transport quantities. Additionally, the effect of collisions between electrons and inelastic effects were neglected, but can be important for more complicated materials and electronic structure.

ACKNOWLEDGMENTS

The authors thank Dr. Louis Jose and Ryan Park for helpful conversations and well as Dr. Charles Starrett for input data. This work is funded by the U.S. Department of Energy NNSA Center of Excellence under cooperative agreement number DE-NA0004146 and by the Department of Energy [National Nuclear Security Administration] University of Rochester “National Inertial Confinement Fusion Program” under award No. DE-NA0004144.

Appendix A: Quantum Scattering

The scheme used for quantum scattering calculations is based in the partial wave expansion [61], where the scattering cross section is expanded in spherical harmonics to give

$$\frac{d\sigma}{d\Omega} = \left| \sum_{l=0}^{\infty} (2l+1) \left(\frac{e^{i\delta_l} \sin \delta_l}{k} \right) P_l(\cos \theta) \right|^2, \quad (\text{A1})$$

where l is the angular momentum quantum number, δ_l is the phase shift, θ is the polar scattering angle, k is the magnitude of scattering k-vector defined using the energy of the scattering event $E = \hbar^2 k^2 / (2m_e)$, and $P_l(x)$ is a Legendre polynomial. Usually, δ_l is determined by solving the radial Schrodinger equation, which can be prone to errors at large energies. Instead the variable phase method [77] is used. This involves solving a non-linear

first order differential equation for the scattering phase shift (given in atomic units $\hbar = m_e = 1$) by

$$\frac{d\delta_l}{dr}(r) = -\frac{2}{k}V(r)\left(\hat{j}_l(kr)\cos\delta_l(r) - \hat{n}_l(kr)\sin\delta_l(r)\right)^2, \quad (\text{A2})$$

where $\delta_l(r)$ is the phase accumulated by a scattered wave function a radius r away from the scattering center, k is the magnitude of the scattering k-vector, and $\hat{j}_l(kr)$ and $\hat{n}_l(kr)$ are Riccati-Bessel functions defined as $\hat{j}_l(kr) = krj_l(kr)$ and $\hat{n}_l = krn_l(kr)$ where $j_l(kr)$ and $n_l(kr)$ are the usual spherical Bessel functions. This equation has the initial condition that $\delta_l(0) = 0$ and must be integrated to a distance that the potential $V(r)$ is sufficiently small so that the system can be considered to be in its asymptotic state.

The phase equation Eq. (A2) can be a stiff differential equation, so special solvers must be used. One such solver which has proven robust in this problem is LSODA [78]. At higher temperatures, when hundreds of partial waves are required for convergence, the scheme is changed from solving Eq. (A2) to using a Born approximation for the phase shift given by [56]

$$\delta_l = -\frac{2}{k} \int_0^\infty dr V(r) \left(\hat{j}_l(kr)\right)^2. \quad (\text{A3})$$

The switch between Eq. (A2) and Eq. (A3) is explained in Ref. [56], and involves predicting when the scattered wave functions will have non trivial features the Born-type approximation cannot capture.

At even larger energies, when $\max(rV(r)) < \gamma\hbar^2k^2/(2m_e)$, the full Born cross section is used for the entire calculation [61]

$$\frac{d\sigma}{d\Omega} = \left| -\frac{2}{q} \int_0^\infty dr r V(r) \sin(qr) \right|^2 \quad (\text{A4})$$

where $q = 2k \sin(\theta/2)$, and γ is a constant usually set to 0.07.

Finally, often the differential cross section can be separated from all the other integrals and can be put into the momentum transfer cross section defined as

$$\sigma_p = \int d\Omega \frac{d\sigma}{d\Omega} (1 - \cos\theta). \quad (\text{A5})$$

This can be expanded with Legendre polynomials and reduced in the partial wave expansion to

$$\sigma_p = \frac{4\pi}{k^2} \sum_{l=0}^{\infty} (l+1) \sin^2(\delta_{l+1} - \delta_l) \quad (\text{A6})$$

where k is the k-vector of a collision, l is the angular momentum quantum number and δ_l is the phase shift for a scattered wave with angular momentum l .

Appendix B: Reference Frame for Numerical Calculations

When deriving Eq. (12) from Eq. (10), one must choose a reference frame for numerical integration. This is fairly complicated as there are three vectors which must be explicitly written out, and none of them share a convenient form. The three vectors are the pre-collision relative velocity \mathbf{u} , the change in the relative velocity over the collision $\Delta\mathbf{u}$, and the ion velocity in the frame of reference of electrons $\Delta\mathbf{V}$. Since the only free vector here is the ion velocity, this is chosen as the z-axis for the integration. The pre-collision relative velocity vector in spherical co-ordinates is $\mathbf{u} = u[\sin\theta' \cos\phi' \hat{x} + \sin\theta' \sin\phi' \hat{y} + \cos\theta' \hat{z}]$ where $u = |\mathbf{u}|$. The change in the relative velocity vector is then the complicated one, as it is related to \mathbf{u} by the scattering angles θ and ϕ . It is given by

$$\begin{aligned} \Delta\mathbf{u} = u & \left[\cos\phi'(\sin\theta \cos\theta' \cos(\phi - \phi') - \sin\theta \tan\phi' \sin(\phi - \phi') + (\cos\theta - 1) \sin\theta') \hat{x} \right. \\ & + \sin\phi'(\sin\theta \cos\theta' \cos(\phi - \phi') + \sin\theta \cot\phi' \sin(\phi - \phi') + (\cos\theta - 1) \sin\theta') \hat{y} \\ & \left. + ((\cos\theta - 1) \cos\theta' - \sin\theta' \sin\theta \cos(\phi - \phi')) \hat{z} \right]. \end{aligned} \quad (\text{B1})$$

The utility in defining $\tilde{\phi} = \phi - \phi'$ can now be explicitly seen. It can also be recognized that the integral over ϕ' in Eq. (10) will cause the x and y components of the

expression to go to 0, due to the $\cos\phi'$ and $\sin\phi'$ terms, indicating that the stopping force is along the velocity of the ballistic particle.

[1] H. Bethe, Zur theorie des durchgangs schneller korpuskularstrahlen durch materie, *Annalen der Physik* **397**, 325

(1930).

- [2] J. Ziegler and J. Manoyan, The stopping of ions in compounds, Nuclear Instruments and Methods in Physics Research Section B: Beam Interactions with Materials and Atoms **35**, 215 (1988).
- [3] R. Betti and O. A. Hurricane, Inertial-confinement fusion with lasers, Nature Physics **12**, 435 (2016).
- [4] A. B. Zylstra and O. A. Hurricane, On alpha-particle transport in inertial fusion, Physics of Plasmas **26**, 062701 (2019).
- [5] M. Key, S. Hatchett, A. Mackinnon, P. Patel, R. Snavely, and R. Stephens, Proton fast ignition, Fusion Science and Technology **49** (2005).
- [6] A. B. Zylstra, J. A. Frenje, P. E. Grabowski, C. K. Li, G. W. Collins, P. Fitzsimmons, S. Glenzer, F. Graziani, S. B. Hansen, S. X. Hu, M. G. Johnson, P. Keiter, H. Reynolds, J. R. Rygg, F. H. Séguin, and R. D. Petrasso, Measurement of charged-particle stopping in warm dense plasma, Phys. Rev. Lett. **114**, 215002 (2015).
- [7] W. Cayzac, V. Bagnoud, M. M. Basko, A. Blažević, A. Frank, D. O. Gericke, L. Hallo, G. Malka, A. Ortner, A. Tauschwitz, J. Vorberger, and M. Roth, Predictions for the energy loss of light ions in laser-generated plasmas at low and medium velocities, Phys. Rev. E **92**, 053109 (2015).
- [8] W. Cayzac, A. Frank, A. Ortner, V. Bagnoud, M. M. Basko, S. Bedacht, C. Bläser, A. Blažević, S. Busold, O. Deppert, J. Ding, M. Ehret, P. Fiala, S. Frydrych, D. O. Gericke, L. Hallo, J. Helfrich, D. Jahn, E. Kjar-tansson, A. Knetsch, D. Kraus, G. Malka, N. W. Neumann, K. Pépitone, D. Pepler, S. Sander, G. Schaumann, T. Schlegel, N. Schroeter, D. Schumacher, M. Seibert, A. Tauschwitz, J. Vorberger, F. Wagner, S. Weih, Y. Zobus, and M. Roth, Experimental discrimination of ion stopping models near the bragg peak in highly ionized matter, Nature Communications **8**, 15693 (2017).
- [9] J. A. Frenje, R. Florido, R. Mancini, T. Nagayama, P. E. Grabowski, H. Rinderknecht, H. Sio, A. Zylstra, M. Gatu Johnson, C. K. Li, F. H. Séguin, R. D. Petrasso, V. Y. Glebov, and S. P. Regan, Experimental validation of low- z ion-stopping formalisms around the bragg peak in high-energy-density plasmas, Phys. Rev. Lett. **122**, 015002 (2019).
- [10] A. C. Hayes, M. E. Gooden, E. Henry, G. Jungman, J. B. Wilhelmy, R. S. Rundberg, C. Yeaman, G. Kyrala, C. Cerjan, D. L. Danielson, J. Daligault, C. Wilburn, P. Volegov, C. Wilde, S. Batha, T. Bredeweg, J. L. Kline, G. P. Grim, E. P. Hartouni, D. Shaughnessy, C. Velsko, W. S. Cassata, K. Moody, L. F. Berzak Hopkins, D. Hinkel, T. Döppner, S. Le Pape, F. Graziani, D. A. Callahan, O. A. Hurricane, and D. Schneider, Plasma stopping-power measurements reveal transition from non-degenerate to degenerate plasmas, Nature Physics **16**, 432 (2020).
- [11] S. Malko, W. Cayzac, V. Ospina-Bohórquez, K. Bhutwala, M. Bailly-Grandvaux, C. McGuffey, R. Fedosejevs, X. Vaisseau, A. Tauschwitz, J. I. Apiñaniz, D. De Luis Blanco, G. Gatti, M. Huault, J. A. Perez Hernandez, S. X. Hu, A. J. White, L. A. Collins, K. Nichols, P. Neumayer, G. Faussurier, J. Vorberger, G. Prestopino, C. Verona, J. J. Santos, D. Batani, F. N. Beg, L. Roso, and L. Volpe, Proton stopping measurements at low velocity in warm dense carbon, Nat. Commun. **13**, 2893 (2022).
- [12] B. Lahmann, A. M. Saunders, T. Döppner, J. A. Frenje, S. H. Glenzer, M. Gatu-Johnson, G. Sutcliffe, A. B. Zylstra, and R. D. Petrasso, Measuring stopping power in warm dense matter plasmas at omega, Plasma Physics and Controlled Fusion **65**, 095002 (2023).
- [13] E. A. Uehling and G. E. Uhlenbeck, Transport phenomena in einstein-bose and fermi-dirac gases. i, Phys. Rev. **43**, 552 (1933).
- [14] E. A. Uehling, Transport phenomena in einstein-bose and fermi-dirac gases. ii, Phys. Rev. **46**, 917 (1934).
- [15] J.-P. Hansen and I. R. McDonald, *Theory of Simple Liquids*, 4th ed. (Oxford: Academic Press, 2013).
- [16] C. E. Starrett and D. Saumon, Electronic and ionic structures of warm and hot dense matter, Phys. Rev. E **87**, 013104 (2013).
- [17] C. Starrett, Potential of mean force for electrical conductivity of dense plasmas, High Energy Density Physics **25**, 8 (2017).
- [18] S. D. Baalrud and J. Daligault, Effective potential theory for transport coefficients across coupling regimes, Phys. Rev. Lett. **110**, 235001 (2013).
- [19] S. D. Baalrud and J. Daligault, Mean force kinetic theory: A convergent kinetic theory for weakly and strongly coupled plasmas, Physics of Plasmas **26**, 082106 (2019).
- [20] S. Rightley and S. D. Baalrud, Kinetic model for electron-ion transport in warm dense matter, Phys. Rev. E **103**, 063206 (2021).
- [21] L. Spitzer, *Physics of Fully Ionized Gases*, 2nd ed. (Interscience Publishers, 1962).
- [22] Y. T. Lee and R. M. More, An electron conductivity model for dense plasmas, The Physics of Fluids **27**, 1273 (1984).
- [23] C.-K. Li and R. D. Petrasso, Charged-particle stopping powers in inertial confinement fusion plasmas, Phys. Rev. Lett. **70**, 3059 (1993).
- [24] L. S. Brown, D. L. Preston, and R. L. Singleton Jr., Charged particle motion in a highly ionized plasma, Physics Reports **410**, 237 (2005).
- [25] D. Nicholson, *Introduction to Plasma Theory*, 1st ed. (Wiley, 1983).
- [26] G. Zwicknagel, C. Toepffer, and P.-G. Reinhard, Stopping power of heavy ions in strongly coupled plasmas, Laser and Particle Beams **13**, 311–319 (1995).
- [27] P. E. Grabowski, M. P. Surh, D. F. Richards, F. R. Graziani, and M. S. Murillo, Molecular dynamics simulations of classical stopping power, Phys. Rev. Lett. **111**, 215002 (2013).
- [28] D. J. Bernstein, S. D. Baalrud, and J. Daligault, Effects of coulomb coupling on stopping power and a link to macroscopic transport, Physics of Plasmas **26**, 082705 (2019).
- [29] A. Schleife, Y. Kanai, and A. A. Correa, Accurate atomistic first-principles calculations of electronic stopping, Phys. Rev. B **91**, 014306 (2015).
- [30] R. J. Magyar, L. Shulenburger, and A. D. Baczewski, Stopping of deuterium in warm dense deuterium from ehrenfest time-dependent density functional theory, Contributions to Plasma Physics **56**, 459 (2016).
- [31] Y. H. Ding, A. J. White, S. X. Hu, O. Certik, and L. A. Collins, Ab initio studies on the stopping power of warm dense matter with time-dependent orbital-free density functional theory, Phys. Rev. Lett. **121**, 145001 (2018).
- [32] A. J. White, O. Certik, Y. H. Ding, S. X. Hu, and L. A. Collins, Time-dependent orbital-free density functional theory for electronic stopping power: Comparison to the

- mermin-kohn-sham theory at high temperatures, *Phys. Rev. B* **98**, 144302 (2018).
- [33] A. J. White, L. A. Collins, K. Nichols, and S. X. Hu, Mixed stochastic-deterministic time-dependent density functional theory: application to stopping power of warm dense carbon, *Journal of Physics: Condensed Matter* **34**, 174001 (2022).
- [34] A. Kononov, T. W. Hentschel, S. B. Hansen, and A. D. Baczewski, Trajectory sampling and finite-size effects in first-principles stopping power calculations, *npj Computational Materials* **9**, 205 (2023).
- [35] A. Kononov, A. J. White, K. A. Nichols, S. X. Hu, and A. D. Baczewski, Reproducibility of real-time time-dependent density functional theory calculations of electronic stopping power in warm dense matter, *Physics of Plasmas* **31**, 043904 (2024).
- [36] G. Zwicknagel, Theory and simulation of heavy ion stopping in plasma, *Laser and Particle Beams* **27**, 399–413 (2009).
- [37] G. Zwicknagel, C. Toepffer, and P.-G. Reinhard, Stopping of heavy ions in plasmas at strong coupling, *Physics Reports* **309**, 117 (1999).
- [38] D. O. Gericke and M. Schlages, Beam-plasma coupling effects on the stopping power of dense plasmas, *Phys. Rev. E* **60**, 904 (1999).
- [39] D. O. Gericke, M. S. Murillo, and M. Schlages, Dense plasma temperature equilibration in the binary collision approximation, *Phys. Rev. E* **65**, 036418 (2002).
- [40] D. O. Gericke and M. Schlages, Energy deposition of heavy ions in the regime of strong beam-plasma correlations, *Phys. Rev. E* **67**, 037401 (2003).
- [41] J. Daligault, On the quantum landau collision operator and electron collisions in dense plasmas, *Physics of Plasmas* **23**, 032706 (2016).
- [42] J. Daligault, Collisional transport coefficients of dense high-temperature plasmas within the quantum landau-fokker-planck framework, *Physics of Plasmas* **25**, 082703 (2018).
- [43] N. R. Shaffer and C. E. Starrett, Model of electron transport in dense plasmas spanning temperature regimes, *Phys. Rev. E* **101**, 053204 (2020).
- [44] J. Lindhard, Motion of swift charged particles, as influenced by strings of atoms in crystals, *Physics Letters* **12**, 126 (1964).
- [45] N. D. Mermin, Lindhard dielectric function in the relaxation-time approximation, *Phys. Rev. B* **1**, 2362 (1970).
- [46] T. A. Mehlhorn, A finite material temperature model for ion energy deposition in ion-driven inertial confinement fusion targets, *Journal of Applied Physics* **52**, 6522 (1981).
- [47] P. Wang, T. M. Mehlhorn, and J. J. MacFarlane, A unified self-consistent model for calculating ion stopping power in icf plasma, *Physics of Plasmas* **5**, 2977 (1998).
- [48] Z. A. Moldabekov, T. Dornheim, M. Bonitz, and T. S. Ramazanov, Ion energy-loss characteristics and friction in a free-electron gas at warm dense matter and non-ideal dense plasma conditions, *Phys. Rev. E* **101**, 053203 (2020).
- [49] T. W. Hentschel, A. Kononov, A. Olmstead, A. Cangi, A. D. Baczewski, and S. B. Hansen, Improving dynamic collision frequencies: Impacts on dynamic structure factors and stopping powers in warm dense matter, *Physics of Plasmas* **30**, 062703 (2023).
- [50] L. Boltzmann, Further studies on the thermal equilibrium of gas molecules, in *The Kinetic Theory of Gases* (1872) pp. 262–349.
- [51] J. Daligault, S. D. Baalrud, C. E. Starrett, D. Saumon, and T. Sjostrom, Ionic transport coefficients of dense plasmas without molecular dynamics, *Phys. Rev. Lett.* **116**, 075002 (2016).
- [52] J. Daligault, Crossover from classical to fermi liquid behavior in dense plasmas, *Phys. Rev. Lett.* **119**, 045002 (2017).
- [53] W. H. Barkas, J. N. Dyer, and H. H. Heckman, Resolution of the Σ^- -mass anomaly, *Phys. Rev. Lett.* **11**, 26 (1963).
- [54] M. Bonitz, *Quantum Kinetic Theory*, 2nd ed. (Springer Cham, 2016).
- [55] D. B. Boercker and J. W. Dufty, Degenerate quantum gases in the binary collision approximation, *Annals of Physics* **119**, 43 (1979).
- [56] C. Lin, B. He, Y. Wu, and J. Wang, A new efficient approach for the calculation of cross-sections with application to yukawa potential, *Plasma Physics and Controlled Fusion* **65**, 055005 (2023).
- [57] L. G. Stanton and M. S. Murillo, Ionic transport in high-energy-density matter, *Phys. Rev. E* **93**, 043203 (2016).
- [58] P. A. M. Dirac, Note on exchange phenomena in the thomas atom, *Mathematical Proceedings of the Cambridge Philosophical Society* **26**, 376–385 (1930).
- [59] C. E. Starrett, T. Q. Thelen, C. J. Fontes, and D. A. Rehn, Excited states in warm and hot dense matter, *Phys. Rev. E* **109**, 035201 (2024).
- [60] R. Betti, A. Christopherson, A. Bose, and K. Woo, Alpha heating and burning plasmas in inertial confinement fusion, *Journal of Physics: Conference Series* **717**, 012007 (2016).
- [61] J. Sakurai and J. Napolitano, *Modern Quantum Mechanics*, 3rd ed. (Cambridge University Press, 2021).
- [62] F. Reif, *Fundamentals of Statistical and Thermal Physics* (McGraw-Hill, 1965).
- [63] C. Cercignani, *Mathematical Methods in Kinetic Theory*, 1st ed. (Springer, 1969).
- [64] J. H. Ferziger and H. G. Kaper, *Mathematical Theory of Transport Processes in Gases* (American Elsevier and North-Holland, 1972).
- [65] B. M. Haines, Charged particle transport coefficient challenges in high energy density plasmas, *Physics of Plasmas* **31**, 050501 (2024).
- [66] P. Hohenberg and W. Kohn, Inhomogeneous electron gas, *Phys. Rev.* **136**, B864 (1964).
- [67] W. Kohn and L. J. Sham, Self-consistent equations including exchange and correlation effects, *Phys. Rev.* **140**, A1133 (1965).
- [68] N. D. Mermin, Thermal properties of the inhomogeneous electron gas, *Phys. Rev.* **137**, A1441 (1965).
- [69] A. D. Baczewski, L. Shulenburger, M. P. Desjarlais, S. B. Hansen, and R. J. Magyar, X-ray thomson scattering in warm dense matter without the chihara decomposition, *Phys. Rev. Lett.* **116**, 115004 (2016).
- [70] R. P. Feynman, N. Metropolis, and E. Teller, Equations of state of elements based on the generalized fermi-thomas theory, *Phys. Rev.* **75**, 1561 (1949).
- [71] M. Lampe, Transport coefficients of degenerate plasma, *Phys. Rev.* **170**, 306 (1968).
- [72] M. Zaghoo, T. R. Boehly, J. R. Rygg, P. M. Celliers, S. X. Hu, and G. W. Collins, Breakdown of fermi degeneracy in

- the simplest liquid metal, *Phys. Rev. Lett.* **122**, 085001 (2019).
- [73] N. W. Ashcroft and N. D. Mermin, *Solid State Physics* (Harcourt, 1976).
- [74] A. Sommerfeld, Zur elektronentheorie der metalle auf grund der fermischen statistik, *Zeitschrift für Physik* **27**, 1 (1928).
- [75] N. R. Shaffer and S. D. Baalrud, The barkas effect in plasma transport, *Physics of Plasmas* **26**, 032110 (2019).
- [76] L. Jose, D. J. Bernstein, and S. D. Baalrud, Barkas effect in strongly magnetized plasmas, *Physics of Plasmas* **29**, 112103 (2022).
- [77] F. Calogero, *Variable Phase Approach to Potential Scattering* (Elsevier, 1967).
- [78] A. Hindmarsh and L. Petzold, *Lsoda*, ordinary differential equation solver for stiff or non-stiff system (2005).